PHYSICAL REVIEW B VOLUME 17, NUMBER 2 15 JANUARY 1978

Self-consistent LCAO calculation of the electronic properties of graphite. I. The regular graphite lattice

Alex Zunger*
Department of Theoretical Physics and Applied Mathematics, Soreq Nuclear Research Centre, Yavne, Israel
(Received 11 August 1975)

The electronic properties of the regular graphite lattice are investigated within self-consistent LCAO (linear combination of atomic orbitals) scheme based as a modified extended-Hückel approximation. The band structure and interband transition energies agree favorably with previous first-principles calculations. Good agreement with experimental data on the density of valence states, energetic position of the lowest conduction states, equilibrium unit-cell parameters, cohesive energy and vibration force constants, is obtained. The McClure band parameters that were previously adjusted to obtain agreement with Fermi-surface data and the electronic specific heat, are reasonably reproduced. The charge distribution and bonding characteristics of the covalent graphite structure, are discussed. The same calculation scheme is used in part II of this article (following paper) to discuss properties associated with point defects in graphite. The correlation between the electronic properties of the regular and point-defect-containing lattice is studied.

I. INTRODUCTION

In view of the accumulation of rather detailed experimental data on the electronic properties of both regular and point-defect containing semiconducting covalent solids, theoretical interest has developed in methods that are capable of treating these related phenomena by a unified approach. The electronic properties of point defects in covalent solids have been treated either by methods using the perfect-lattice periodic states as zero-order eigenvectors[1-5] or by methods that have utilized the local atomic orbitals surrounding the defect site to construct the "defect molecule."[6-8] The first approach, usually implemented either by using various forms of resolvent methods[1-4] or by direct expansion techniques,[5] does not provide a natural way of introducing self-consistency in the description of the charge rearrangement accompanying the defect formation, and in many cases requires the knowledge of the perfect-crystal eigenstates in the Wannier representation. Lattice distortions around the defect site are usually not amenable to treatment by these methods owing to the large perturbation associated with such a rearrangement. The second approach, using the defects local-environment representation, does not provide a correlative scheme between the eigenvalue spectrum associated with the defect and the perfect-solid band structure, and is deficient both in the description of the coupling of the defect states with the band states and in treating the relaxation of the lattice. Effective-mass theories[9,10] on the other hand, are not suitable for description of deep defect levels associated with a deep short-range potential, since in these systems, a rather substantial part of the Brillouin zone (BZ) and more than a single band are important in determining the defect levels. Truncated-crystal calculations[11-13] solving for the eigenvalue problem of a relatively large cluster of atoms with a defect placed at its center, have yielded a wealth of information regarding the charge distribution around the defect and the relaxation mechanisms; however, owing to the presence of a substantial number of dangling bonds on the cluster's surface, significant unrealistic charge inhomogeneity is generated in the cluster. Except for clusters with special symmetries,[13] one cannot establish a correlation between the cluster's energy eigenvalues and those of the perfect infinite solid.[14]

Recently, a new model has been suggested[14-18] for treating point defects in covalent solids. This model is based on the representation of the one-electron energies of the defect by the eigenvalue spectrum of a small *periodic* cluster of atoms treated in the LCAO (linear combination of atomic orbitals) representation. Undesired surface effects are completely eliminated and a simple correspondence between the cluster levels and that of the infinite solid is established. Lattice relaxations can be conveniently treated and coupling of the defect states with the bulk crystal bands at a discrete subset of points in the BZ is automatically introduced. In the present paper we treat the electronic structure of the perfect lattice and in part II[19] (following paper) we treat the vacancy problem in graphite using this "small-periodic-cluster" (SPC) approach. We extend our previous treatment of point defects in hexagonal systems[17,18] by introducing recently developed theorems[20,21] for the mean value points in the BZ in conjunction with the small-periodic-cluster

approach, enabling a detailed study of self-consistency effects and emphasizing the density-of-states aspects of the problem. Both the localized and the extended crystal states in the presence of the vacancy are examined.

The problem of describing the electronic states of perfect lattice and radiation-damage induced defects in graphite, is one of great importance, both from the fundamental and practical point of view. In the past years, a large amount of experimental data concerning the electronic structure of both the perfect and the defect structure has been accumulated. The perfect lattice has been studied by optical absorption,[22] reflectance,[23-26] electron energy loss,[27,28] thermoreflectance,[29] soft-x-ray emission,[30] photoelectron spectroscopy (ESCA),[31-34] secondary-electron emission (SEE),[35,36] and photoemission.[35] The details of the Fermi surface have been analyzed by the de Haas–Van Alphen effect,[37,38] cyclotron resonance,[39,40] and magnetoreflectance.[41] Electronic heat capacity has been measured and analyzed by several authors.[42-44] The crystal force constants have been deduced[45,46] from neutron-scattering data[47] by fitting the calculated phonon spectra to experiment while the lattice sublimation energy has been measured by thermochemical techniques.[48-50] The properties associated with point vacancies in graphite have also received experimental attention. Experiments on electron paramagnetic resonance of damaged-graphite[51-53] lattice-parameter change due to defect formation[54-56] and displacement energy by electron impact[57-59] have been performed. Optical absorption of irradiated graphite,[60] diffusion, thermal-annealing, and stored-energy-release experiments measuring the energy of vacancy formation and migration[61-65] have been performed. The electron dynamics in the presence of defects has been examined by Hall-effect experiments,[66] magnetoresistivity,[66,67] and electrical resistivity.[68]

Theoretical studies on the electronic properties of graphite have been performed both within the π-electron approximation[69-73] and within the all-valence electron model.[17,74-81] The electronic structure of the point vacancy in the same system has been treated by the nearest-neighbor "defect molecule" approach.[7]

In this paper (part I) we treat the electronic band structure of graphite within the LCAO tight-binding scheme using a self-consistent modification to the extended-Hückel (EXH)[82] approximation to the interaction integrals. It has been previously indicated[17,18,83-86] that a charge-self-consistent scheme is essential for maintaining realistic description of systems exhibiting some sort of heteropolarity, such as binary crystals[83-86] or homopolar crystals containing defects.[17] There is some strong evidence[87-89] that for systems with relatively homogeneous charge distribution (e.g., homopolar molecules and solids or systems with small electronegativity difference between the constituent atoms), the EXH method provides a reasonable approximation to the Hartree-Fock–Roothaan method.

The details of the calculations involved in EXH band structure are described in Sec. II and in Sec. III we discuss the results of optical transitions, positions of high-symmetry points with respect to the Fermi energy, electron density of states, imaginary part of the dielectric function, valence-charge distribution, unit-cell parameters, force constants, and various band parameters related to Fermi-surface data. Comparisons with both available experimental data and with other theoretical approaches are discussed. In the second article (part II), we use the self-consistent EXH method in a small-periodic-cluster approach to calculate various properties related to the vacancy in graphite, i.e., energy of localized states, density of states in the presence of the vacancy, Jahn–Teller distortions, energy of vacancy formation, and migration and charge redistribution due to the defect. A completely self-consistent approach is used. Relations with previous approaches and with available experimental data are discussed in detail.

II. METHOD OF CALCULATION

The Bloch function $\Phi_\mu^\alpha(\vec{k},\vec{r})$ constructed from atomic orbital $\chi_\mu(\mu=1,\ldots,\sigma)$ situated at the site $\alpha(\alpha=1,\ldots,h)$ in the unit cell is given by

$$\Phi_\mu^\alpha(\vec{k},\vec{r}) = N^{-1/2}\sum_n e^{i\vec{k}\cdot\vec{R}_n}\chi_\mu(\vec{r}-\vec{R}_n-\vec{d}_\alpha), \tag{1}$$

where $n=1,\ldots,N$ numbers the unit cells and $\vec{d}_\alpha$ is the position vector of site α in the unit cell. Crystal eigenfunctions belonging to the jth band $(j=1,\ldots,\sigma h)$ are given by

$$\Psi_j(\vec{k},\vec{r}) = \sum_{\mu=1}^{\sigma}\sum_{\alpha=1}^{h} C_{\mu j}^\alpha(\vec{k})\,\Phi_\mu^\alpha(\vec{k},\vec{r}). \tag{2}$$

The expansion coefficients $C_{\mu j}^\alpha(\vec{k})$ and the band eigenvalues $\epsilon_j(\vec{k})$ are determined from the solution of the variational equations:

$$\sum_{\mu=1}^{\sigma}\sum_{\alpha=1}^{h}[F_{\mu\nu}^{\alpha\beta}(\vec{k}) - S_{\mu\nu}^{\alpha\beta}(\vec{k})\epsilon_j(\vec{k})]C_{\mu j}^\alpha(\vec{k}) = 0. \tag{3}$$

The matrix elements of the Bloch function are given in the atomic basis set by

$$F^{\alpha\beta}_{\mu\nu}(\vec{k}) = \sum_m e^{i\vec{k}\cdot(\vec{R}_m - \vec{R}_0)} \times \langle \chi_\mu(\vec{r} - \vec{R}_0 - \vec{d}_\alpha) | \hat{F} | \chi_\nu(\vec{r} - \vec{R}_m - \vec{d}_\beta) \rangle \equiv \sum_n e^{i\vec{k}\cdot\vec{R}_n} F^{\alpha\beta}_{\mu\nu}(0,n),$$
$$S^{\alpha\beta}_{\mu\nu}(\vec{k}) = \sum_m e^{i\vec{k}\cdot(\vec{R}_m - \vec{R}_0)} \times \langle \chi_\mu(\vec{r} - \vec{R}_0 - \vec{d}_\alpha) | \chi_\nu(\vec{r} - \vec{R}_m - \vec{d}_\beta) \rangle \equiv \sum_n e^{i\vec{k}\cdot\vec{R}_n} S^{\alpha\beta}_{\mu\nu}(0,n), \quad (4)$$

where $\vec{R}_0$ is the position vector of the origin unit cell and $F^{\alpha\beta}_{\mu\nu}(0,n)$ and $S^{\alpha\beta}_{\mu\nu}(0,n)$ are the matrix elements of the Hartree-Fock operator $\hat{F}$ and the unity operator, respectively.

The secular equations [Eq. (3)] are solved by applying the Löwdin orthogonal transformation[90] to the basis Bloch functions followed by a direct diagonalization of the orthogonal eigenvalue equations. The resulting wave functions are subjected to a Löwdin charge analysis.[90] The elements of the charge matrix are computed by replacing the Brillouin zone integration by a numerical quadrature[91] over 180 inequivalent $\vec{k}$ points in the $\frac{1}{12}$ section of the two-dimensional hexagonal Brillouin zone. The population analysis is used to compute the following quantities: (a) the charge contribution by the μ-basis orbital to the state $|\vec{k}j\rangle$. The dispersion curves of this orbital charge $q^\alpha_\mu(\vec{k}j)$ is calculated for all occupied bands, through the Brillouin zone. (b) A band-by-band integration of $q^\alpha_\mu(\vec{k},j)$ yields the contribution of the jth band to the μ-orbital charge $R^\alpha_{\mu j}$. (c) The contribution of the jth band to the total electronic charge on site α, D^α_j is computed by summing $R^\alpha_{\mu j}$ over the basis orbitals μ. The quantity D^α_j for the defect level j will be used as a measure to the localization of the defect wave function on given sites α. (d) The total electronic charge on site α due to all occupied bands, Q_α. If no charge transfer occurs between the various sublattices, this equals the valence electronic charge of the free atom. (e) The net atomic charge q_α is given by the difference between Q_α and the core charge Z_α. These quantities are defined in Appendix A.

We have used the Löwdin definition of atomic charges rather than the Mulliken[92] or the Ros and Schmit[93] definitions since the latter methods involve a somewhat artificial division of the overlap charge between nonequivalent atoms. This complication does not arise when orthogonal Löwdin functions are used. In systems exhibiting a nonhomogeneous charge distribution (such as heteronuclear solids and molecules or homonuclear systems with point defects), the Löwdin definition has been shown to better reproduce accurately calculated molecular multipoles[94-96] and energies.[97]

The overlap matrix elements $S^{\alpha\beta}_{\mu\nu}(0,n)$ are calculated directly from a valence basis set ($\mu = 2s$, $2p_x$, $2p_y$, and $2p_z$) of Slater orbitals using standard Slater exponents (1.625 for carbon). The energy matrix elements are calculated from a self-consistent extended-Hückel approach, similar to the approximation previously suggested for molecules[98-100]

$$F^{\alpha\beta}_{\mu\nu}(n,m) = \tfrac{1}{2} G_{\mu\nu}[F^{\alpha\alpha}_{\mu\mu}(q_\alpha) + F^{\beta\beta}_{\nu\nu}(q_\beta)] S^{\alpha\beta}_{\mu\nu}(n,m), \quad (5)$$

where $G_{\mu\nu}$ is the Wolfsberg–Helmholz constant.[101] The diagonal $F^{\alpha\alpha}_{\mu\mu}(q_\alpha)$ element is given by:

$$F^{\alpha\alpha}_{\mu\mu}(q_\alpha) = F^\alpha_\mu(0) - q_\alpha \Delta^\mu_{n\alpha,\,n\alpha} - \sum_{l\beta \neq n\alpha} q_\beta \gamma_{n\alpha,\,l\beta}. \quad (6)$$

$F^\alpha_\mu(0)$ is the μ-orbital energy of the neutral atom at site α and is obtained from atomic ionization potentials determined spectroscopically[102,103] and $\Delta^\mu_{n\alpha,\,n\alpha}$ is the change in the μ-orbital energy of atom α due to deviation from charge neutrality at this site. $\gamma_{n\alpha,\,l\beta}$ is the two-center spherically averaged Coulomb repulsion integral:

$$\gamma_{n\alpha,\,l\beta} = \langle \chi_{s\alpha}(\vec{r}_1 - \vec{R}_n - \vec{d}_\alpha)\chi_{s\beta}(\vec{r}_2 - \vec{R}_l - \vec{d}_\beta) \left| \frac{1}{r_{12}} \right| \chi_{s\alpha}(\vec{r}_1 - \vec{R}_n - \vec{d}_\alpha)\chi_{s\beta}(\vec{r}_2 - \vec{R}_l - \vec{d}_\beta) \rangle, \quad (7)$$

calculated from the formula listed by Roothaan.[104] We use a spherically averaged Coulomb repulsion rather than calculate the individual orbital repulsion integrals since this averaging has only little effect on the band pattern.[105] The repulsion integral $\gamma_{n\alpha,\,l\beta}$ behaves asymptotically as an electrostatic point charge potential[106] $\sim |\vec{R}_{n\alpha} - \vec{R}_{l\beta}|^{-1}$ and is screened at shorter range.

The diagonal neutral atom orbital energies $F^\alpha_\mu(0)$ appearing in Eq. (6) and taken from atomic Hartree-Fock calculations or from experiment, consists of a carbon 2s term $F^c_{2s}(0)$ and three *degenerate* carbon 2p terms $F^c_{2p_x}(0) = F^c_{2p_y}(0) = F^c_{2p_z}(0)$. The values usually taken for these quantities in quantum-chemical calculations on carbon containing molecules[82,102] are $F^c_{2s}(0) = -19.44$ eV and $F^c_{2p}(0) = -11.40$ eV. In molecular systems having axial symmetry (e.g., acetylene, ethylene) or a reflection plane (e.g., benzene), the threefold degeneracy of the 2p orbitals is

lifted due to the different crystal-field screening in the various axial directions. Penetration effects of an atomic orbital on a given center into the screened field of other nuclei were shown to lower the energy of the planar terms $F^c_{2p_x}(0) = F^c_{2p_y}(0)$ relatively to the out-of-plane term $F^c_{2p_z}(0)$ in aromatic molecules having their σ manifold in the x-y plane.[107] Since a first-principles way of introducing this effect requires a detailed calculation of all penetration and two-electron integrals, it has been previously suggested[107] that such an "atoms-in-molecules" effect could be introduced phenomenologically by splitting the in-plane and out-of-plane orbital energies artificially. Calculations on several organic molecules showed that a splitting of about $\sim 0.3|F^c_{2p}(0)|$ yields satisfactory agreement with experiment regarding the ordering of molecular levels, ionization potentials, and σ-π splitting. In a previous study on graphite[13] such a procedure has indeed yielded satisfactory results. We consequently split the $F^c_{2p}(0)$ element symmetrically around the commonly employed degenerate value of -11.40 eV taking:

$$F^c_{2p_x}(0) = F^c_{2p_y}(0) = -13.11 \text{ eV},$$
$$F^c_{2p_z}(0) = -9.69 \text{ eV}, \tag{8}$$

and the commonly used $2s$ value: $F^c_{2s}(0) = -19.44$ eV. The Wolfgang–Helmholtz constants are taken as[108]:

$$G_{\mu\nu} = \begin{cases} 2.0, & \mu = \nu = p_z; \\ 1.75, & \text{otherwise.} \end{cases} \tag{9}$$

The one-center term $\Delta^{\mu}_{n\alpha,n\alpha}$, [Eq. (6)] can be obtained from empirical interpolation schemes relating the spectroscopically observed atomic ionization potential $F_\mu(q)$ with the net atomic charge, and,[103,106] from Hartree-Fock calculations[109] or can be deduced from the π-electron transitions in benzene.[110] All these estimates yield values around 11.6 ± 1.1 eV. Inclusion of ionic configurations and correlation effects into the Hartree-Fock estimate yields a value of 10.53 eV,[111] while fitting various calculated properties of carbon-containing molecules to experiment, using diagonal matrix elements of the form $F_\mu(q) = F_\mu(0) + \Delta_\mu q$ yields a value of 11 eV.[100] This value is sufficiently close to those yielded by other approximations and it would be consequently used in this work. Calculations on the charged vacancy in graphite (Sec. II) indicated that orbital energies and atomic charges were rather insensitive ($\sim 7\%$ and $\sim 4\%$ for energies and charges, respectively) to changes in $\Delta^{\mu}_{n\alpha,n\alpha}$ between 10 and 12 eV.

Expression (6) for the diagonal element has a simple physical meaning-an electron in orbital μ on atom α has a binding energy $F^{\alpha}_{\mu}(0)$ corresponding to a neutral system, and experiences both a potential due to accumulation of charge on this site and a screened Madelung-type electrostatic potential due to the field on other atoms. In a neutral system ($q_\alpha = 0$), the diagonal element simply reduces to the atomic ionization potential $F^{\alpha}_{\mu}(0)$, as used in the conventional non-self-consistent extended-Hückel method.[82] The inclusion of the two first terms corresponds to the iterative extended Hückel approximation[99,100] while the inclusion of all three terms corresponds to the modified iterative extended Hückel in which screened Madelung effects are introduced.[86,112-114]

To test the adequacy of the employed atomic parameters for graphite, the one-electron energies of the closely related benzene molecule were computed with the same parameters. A carbon-carbon bond length of 1.40 Å and a carbon-hydrogen bond length of 1.10 Å were used. The conventional[82] value for the hydrogen $1s$ orbital energy $F^H_{1s}(0) = -13.6$ eV was used. The energies ϵ_i of the ten valence molecular levels (for which experimental photoelectron data exist) were compared both with experimental data[115,116] ϵ_i^{exp} and with the results of an extended-basis-set Hartree-Fock calculation,[117] performed with the same nuclear geometry. The standard deviation

$$\sigma = \left(\sum_{i=1}^{10} (\epsilon_i^{\text{calc}} - \epsilon_i^{\text{expt}})^2 \Big/ \sum_{i=1}^{10} (\epsilon_i^{\text{expt}})^2 \right)^{1/2}$$

was found to be 0.093 for the present extended-Hückel calculation and 0.150 for the extended basis set Hartree-Fock calculation.

The calculations were performed in the following way: one guesses the elements of the charge matrix (isolated atom values are used as initial guess) and computes the diagonal energy elements [Eq. (6)] up to a maximal interaction range R_c. These are used together with the computed overlap matrix to calculate all the energy elements [Eqs. (4) and (5)] and to solve the eigenvalue problem [Eq. (3)] at a selected grid in $\vec{k}$ space. The eigenvectors are used to calculate a refined charge matrix and orbital charges [Eqs. (A1)–(A10)] and these in turn are employed for the calculation of the energy elements [Eqs. (5) and (6)]. The process is repeated to obtain a constancy in the charge-matrix elements and band energies between successive iterations of less than $10^{-3}e$ and 10^{-4} eV, respectively. Damping of the iteration cycle[118] is used to facilitate the convergence. The iteration cycle converges readily for the case of a perfect lattice of graphite owing to the lack of interatomic charge transfer in the system. Thus, in this system the simple non-iterative extended-

Hückel method yields good results, as previously demonstrated.[13] However, when lattice imperfections are present (see II),[19] iterations towards self-consistency substantially change the final charges and the energy eigenvalue spectrum. In the convergence limit one computes the total energy per atom:

$$\frac{E_t}{N} = \int_{\text{occ. BZ}} d\vec{k} \sum_{j=1}^{\sigma_{occ}} n_j \epsilon_j(\vec{k}). \tag{10}$$

Numerical first and second derivatives of E_t/N with respect to the totally symmetric stretching mode are performed to yield equilibrium carbon–carbon distances and force constant, respectively. The minimization procedure used to obtain the unit cell parameters at static equilibrium is the standard steepest-descent method in which the displacement $\delta\vec{\xi}$ in the vector $\vec{\xi}$ required to approach equilibrium is iteratively determined by

$$\delta\vec{\xi} = -A\nabla_{\vec{\xi}} E_{tot}(\vec{\xi}), \tag{11}$$

where $\vec{\xi}$ is a vector whose components are the structure parameters to be optimized and A is a numerical scaling factor.

The final eigenvectors are used to compute the electronic charge density in the valence bands:

$$\rho(\vec{r}) = \sum_{j=1}^{\sigma_{occ}} \int d\vec{k} \int d\tau_2 \cdots d\tau_N \times \Psi_j^*(\vec{k}, \vec{r}, \ldots, \vec{r}_N)\Psi_j(\vec{k}, \vec{r}, \ldots, \vec{r}_N). \tag{12}$$

This can be expressed by the atomic basis orbitals χ_μ and their expansion coefficients $C_{\mu j}^{\alpha}$ [Eqs. (1) and (2)]. The Slater atomic orbitals are then expanded in a series of Gaussians using the 6-G expansion of Hehre *et al.*[119] The charge density is thus expressed in terms of the coefficients $C_{\mu j}^{\alpha}(\vec{k})$ and products of Gaussians centered on various sites. These multicenter products can be expressed as a sum of Gaussians centered on single intermediate sites.[120] It has been previously shown in molecular calculations[121] that the electrostatic Poisson potential V_{elec} generated by a charge density expressed as a sum of Gaussians, can be analytically calculated directly from the Poisson equation:

$$\nabla^2 V_{elec}(\vec{r}) = -4\pi\rho(\vec{r}). \tag{13}$$

Following this procedure, we calculate the electronic contribution to the electrostatic potential $V_{elec}(\vec{r})$. This is used for obtaining the perturbative potential exerted by the defect (see Part II).

The convergence of the integrals over the BZ [Eqs. (10) and (12)] as a function of the $\vec{k}$ grid used and that of the sums in direct space [Eq. (4)] as a function of the interaction range R_c, was examined. 180 inequivalent $\vec{k}$ points in the $\frac{1}{12}$ irreducible zone were sufficient to obtain converged results for the charge density elements (error less than $10^{-5}\%$) and total energy ($10^{-4}\%$) in a Simpson integration scheme.[91] Using the special $\vec{k}$ points calculated by Cunningham[21] for the irreducible hexagonal BZ by applying the mean-value algorithm of Chadi and Cohen,[20] it was found that the six special points

$$(k_x, k_y) = (\tfrac{2}{9}, 2/9\sqrt{3}), (\tfrac{4}{9}, 4/9\sqrt{3}), (\tfrac{8}{9}, 4/9\sqrt{3}), (\tfrac{2}{3}, 2/9\sqrt{3}), (\tfrac{8}{9}, 4/9\sqrt{3})(\tfrac{10}{9}, 2/9\sqrt{3})$$

with respective weights of $\frac{1}{9}, \frac{1}{9}, \frac{1}{9}, \frac{2}{9}, \frac{2}{9}, \frac{2}{9}$ were already sufficient to obtain an accuracy of 0.2% for the total energy. This remarkable accuracy is further improved when one employs an artificially large unit cell instead of the primitive cell, thus reducing the dispersion of the energy bands. In calculations involving a large unit cell (20–50 atoms instead of two) associated with the defect problem,[19] only the six special points are used. The charge density [Eq. (12)] in the primitive unit cell calculations is computed throughout this work using the 180 $\vec{k}$ points. The lattice sums in direct space [Eq. (4)] are found to converge for $R_c \leq 22$ Å. Since deviations from charge neutrality associated with the defect structure occur only in the vicinity of the defect site, a discrete summation over 22 Å is sufficient to include even all the electrostatic contributions [Eqs. (6) and (7)] and Fourier-transform convergence procedures[122] are not required.

Using the computed band structure, the electronic density of states given by

$$D(\epsilon) = \frac{1}{\Omega} \sum_{j=1}^{\sigma_{occ}} \int d\vec{k}\,\delta(\epsilon - \epsilon_j(\vec{k})) \tag{14}$$

is calculated. 180 $\vec{k}$ points in the $\frac{1}{12}$ irreducible zone are used to generate 10^4 points by means of Lagrangian interpolation. Energy channels of 0.02 eV are used. The joint density of states

$$J_{vc}(\epsilon) = \frac{1}{\Omega} \int d\vec{k}\,\delta(\epsilon - \epsilon_c(\vec{k}) + \epsilon_v(\vec{k})), \tag{15}$$

where $\epsilon_c(\vec{k})$ and $\epsilon_v(\vec{k})$ denote conduction and valence energy bands, respectively, are similarly calculated. Near the discontinuities in $J_{vc}(\epsilon)$ the derivatives of the valence and conduction bands are analytically computed in order to determine the transition energy at critical points. This is done by the algorithm developed by Delhale and Andre.[123] The $\vec{k}$ derivative is given by direct differentiation of Eq. (3):

$$\frac{d\epsilon_j(\vec{k})}{d\vec{k}} = C_j^{\dagger}(\vec{k}) \frac{dF(\vec{k})}{d\vec{k}} C_j(\vec{k}), \quad j = v, c, \tag{16}$$

where

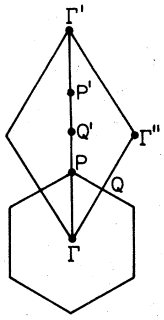

FIG. 1. Two-dimensional Brillouin zone of graphite with the notation for high symmetry points of Lomer (Ref. 74).

$$\frac{dF(\vec{k})}{d\vec{k}} = i\sum_n \vec{R}_n F(0,n) e^{i\vec{k}\cdot\vec{R}_n}.$$

Critical points of interband transition are determined from

$$\nabla_{\vec{k}}[\epsilon_c(\vec{k}) - \epsilon_v(\vec{k})] = 0. \tag{17}$$

In the approximation of constant transition moment for the π and σ bands, the imaginary part of the dielectric function, $\epsilon_2(0,\omega)$ is taken to be proportional to $J_{vc}(\epsilon)/\epsilon^2$.

It should be indicated that although in the two-dimensional graphite structure (with reflection symmetry in the basal plane) the electronic states can be rigorously divided into π and σ states, in our self-consistent calculation scheme, no such separation is invoked. Thus, for instance, Hamiltonian matrix elements coupling π Bloch states are allowed to modify through the self-consistency iteration cycle due to charge rearrangement in *all the occupied* $\sigma+\pi$ *bands* in the Brillouin zone. This is a distinct improvement over both non-self-consistent all-valence electron methods[74-80] and π-electron models.[69-73]

III. RESULTS

A. Band-structure and optical properties

In the two-dimensional graphite structure there are two atoms per unit cell. The primitive translation vectors are $\vec{a}_1 = a(1,0)$ and $\vec{a}_2 = a(\frac{1}{2}, \sqrt{3}/2)$ where the unit cell parameter a, expressed by the carbon-carbon bond length R_0 is $\sqrt{3}R_0$ with $R_0 = 1.42$ Å.[124] The reciprocal lattice vectors are $\vec{b}_1 = (2\pi/a)(1, -1/\sqrt{3})$ and $\vec{b}_2 = (2\pi/a)(0, 2\pi/\sqrt{3})$. The first BZ is a hexagon and is shown in Fig. 1 along with the notation of high symmetry points of Lomer.[74] The symmetry properties of the hexagonal layer structure and the classification of electronic states, have been discussed by Lomer[74] and by Bassani and Parravicini.[76]

Figure 2 shows the results for the band structure along the $\Gamma - P - Q$ lines of the present calculation together with the results of Painter and Ellis[77] and that of Bassani and Parravicini.[76]

Figure 3 shows the band structure obtained by the self-consistent INDO (intermediate neglect of differential overlap) method, similar to the complete neglect of differential overlap (CNDO) method previously used.[80,81] The results of the self-consistent extended-Hückel calculations of the present work [Fig. 2(b)] correspond to the con-

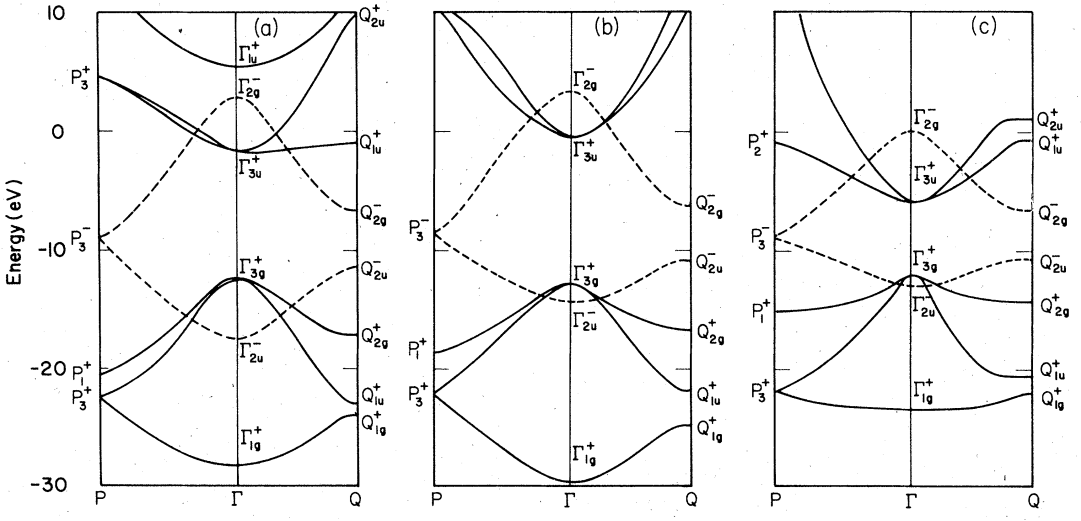

FIG. 2. Band structure of the two-dimensional graphite along the P-Γ-Q directions. (a) Painter and Ellis, Ref. 77; (b) present work, extended Hückel; (c) Bassani and Parravicini, Ref. 76. Full lines constitute the σ bands, the broken lines the π bands. Fermi level is at P_3^-.

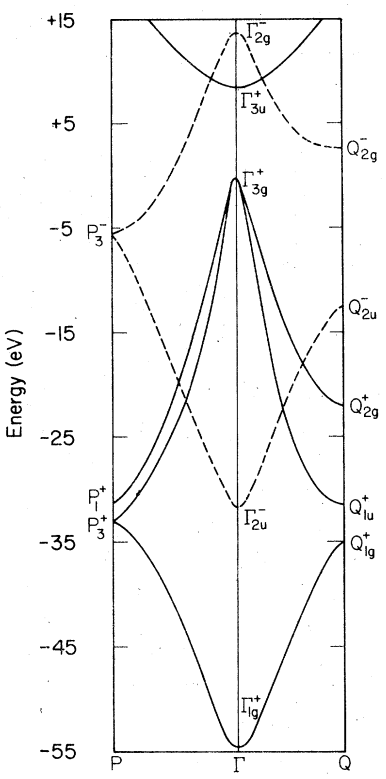

FIG. 3. INDO band structure of the two-dimensional graphite along the P-Γ-Q directions (present work).

vergence limit of both direct and reciprocal space sums, discussed in Sec. II.

In Table I we have compared the theoretically calculated interband transition energies with the experimental reflectance,[23-26] energy loss,[28] photoemission,[35] and secondary-electron-emission[35-36] spectra. Complete assignment of the experimental spectra is still lacking. The lowest $\pi - \pi^*$ transition between the saddle points Q^-_{2u} and Q^-_{2g} states appears to be consistently determined by all workers at around 4.5–4.8 eV, while the lowest $\sigma - \sigma^*$ transition ($\Gamma^+_{3g} - \Gamma^+_{3u}$) has been attributed by Bassani and Parravicini[76] to the weak shoulder observed in the reflectance spectra[25] at 6 eV and by Painter and Ellis[77] to the main reflectance peak at 14.5 eV. It was argued however by the former authors that an artificial increase of the calculated $\sigma \to \sigma^*$ gap from 6 to about 10 eV would yield a better fit with experiment for the calculated $\epsilon_2(0,\omega)$ near the $Q^+_{2g} \to Q^+_{1u}$ transition. Later, SEE[35,36] and photoemission[35] experiments established the onset of the $\sigma \to \sigma^*$ transitions at 11.5 $\pm$0.1 eV.

The results of the present study are in good agreement both with experiment and with the first-principle calculations of Painter and Ellis[77] and Corbato[75] for energies lower than about 10 eV above the Fermi level E_F. Points at higher energy, in the conduction band (i.e., Q^+_{1u} and Q^+_{2u}) are substantially overestimated by the present calculation. In applications of the EXH band structure we will restrict ourselves to energies well below $E_F + 10$ eV.

The pseudopotential calculation[79] yields reasonable results for the main π gap at $Q^-_{2u} - Q^-_{2g}$ and the main σ gap at $\Gamma^+_{3g} - \Gamma^+_{3u}$ but underestimates strongly other transition energies. The order of transitions seems to be incorrectly revealed by this calculation. The INDO band structure (Fig. 3) agrees well with the previously published results of Messmer *et al.*[80] and Kapsomenos[81] using the similar CNDO approximation but disagrees markedly with experimental data (overestimation of the low lying interband transition energies by a factor of 2–3 and of the width of the valence bands by a factor of 3–5).

In previous applications of the CNDO method to band-structure calculations of various carbon-containing organic polymers (see Ref. 123) and references therein), no detailed comparison with experimental optical data was made. Our above conclusions on the inadequacy of the CNDO approximation to graphite and our similar experience on boron nitride,[86] suggests that this might also be a poor approximation for carbon polymers.

Figure 4 shows the imaginary part of the dielectric function perpendicular to the c axis, $\epsilon_{2\perp}(0,\omega)$ as calculated from EXH band structure in the constant oscillator strength approximation. This is compared with the experimentally determined function using reflectivity[23] and electron energy loss[28] data. Only the overall features of the calculated $\epsilon_{2\perp}(0,\omega)$ function could be compared with experiments since the details of the energy dependence of the oscillator strength is not included

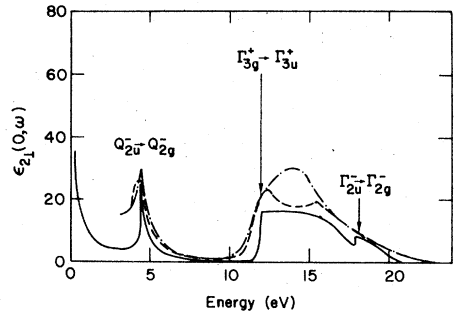

FIG. 4. Experimental and calculated (in arbitrary units) $\epsilon_{2\perp}(0,\omega)$. (——) Calculation; (-.-.-) experimental data from reflectance spectra of Taft and Philipp (Ref. 23); (-----) experimental data from electron energy loss of Tosatti and Bassani (Ref. 28).

TABLE I. Comparison between experimental and calculated interband transitions for graphite. Energies given in eV. $\vec{E}\perp\vec{c}$ and $\vec{E}\parallel\vec{c}$ denote polarization with respect to the c axis.

Transition	Expt. Results	EXH present work	Painter and Ellis [a]	Bassani and Parravicini [b]	Corbato [c]	Tsukada *et al.* [d]	Haeringen [e]
$Q^-_{2u}\rightarrow Q^-_{2g}$ $(\vec{E}\perp\vec{c})$	4.5,[f] 4.8,[g] 4.6,[h] 4.85[i]	4.5	4.7	4.5[j]	5.15	5.14[j]	3.3
$\Gamma^+_{3g}\rightarrow \Gamma^+_{3u}$ $(\vec{E}\perp\vec{c})$	11.50±0.1[k] 11[f]	12.1	12.2	6.0[j]	12.4	···	10.7
$Q^+_{2g}\rightarrow Q^+_{1u}$ $(\vec{E}\perp\vec{c})$	15.0±0.5[k] 14.8[l]	27	16.3	14.0	15.3	···	4.9
$\Gamma^-_{2u}\rightarrow \Gamma^-_{2g}$ $(\vec{E}\perp\vec{c})$	<20,[k] 16[l]	17.2	17.5	13.0	22.4	18.7	8.9
$Q^+_{1u}\rightarrow Q^-_{2g}$ $(\vec{E}\parallel\vec{c})$	15.0[l] 14.5±2[k]	15.8	16.5	13.0	14.2	···	···
$Q^+_{2g}\rightarrow Q^-_{2g}$ $(\vec{E}\parallel\vec{c})$	dipole forbidden	10.4	10.3	7.5	9.0	···	4.3

[a] Discrete variational method, Ref. 77.
[b] Empirical tight binding, Ref. 76.
[c] First-principles LCAO, Ref. 75.
[d] π-orthogonalized-plane-wave, Ref. 73.
[e] Empirical pseudopotential, Ref. 79.
[f] Reflectivity, Ref. 23.
[g] Reflectivity, Ref. 24.
[h] Reflectivity, Ref. 25.
[i] Thermoreflectance, Ref. 29.
[j] Adjusted value.
[k] Secondary electron emission, Ref. 35, 36.
[l] Reflectivity, Ref. 26.

in the calculation. The agreement below the π plasma frequency ($\omega_{p\pi}\cong 7$ eV)[23, 25, 26] is satisfactory. At higher energies the calculated $\epsilon_{2\perp}(0,\omega)$ shows a small shoulder at around 17–18 eV which is absent in the reflectance spectra and seems to appear at about 15–16 eV in the electron energy loss data. Owing to the occurrence of the Q^+_{1u} state at relatively high energy in our calculation, the $Q^+_{2g}\rightarrow Q^+_{1u}$ transition is not contributing much to the calculated $\epsilon_{2\perp}(0,\omega)$ around 15–20 eV in contrast with the results of Bassani and Parravicini.[76]

In Table II we compare the energetic position of some high symmetry points in the conduction band, relative to the theoretical Fermi level E_F (located at the P^-_3 point) with the experimental determination by SEE.[35] With this technique, only energy levels located above the vacuum level ($E_F+\Phi$), where the work function Φ for graphite is 4.7 eV,[125] are determined (e.g., higher than the Γ^+_{3u} level). Since electrons are initially excited into levels in high density-of-state regions in the conduction band and subsequently relaxed due to electron-electron and electron-phonon scattering into lower minima in the energy bands, the energetic positions observed in SEE experiments provide lower bounds. Again, it is observed that the present EXH calculation are in good agreement with experiment for the lowest zone-center conduction-band levels but in rather poor agreement with high-energy zone-edge antibonding levels.

B. Density of states

The partial density of states of graphite is shown in Fig. 5 together with the notation for special points. Saddle-point singularities occur at the Q point while the P point creates local minima in the density of states. Since a detailed density of states has not been published previously, only the gross features of the present calculation can be compared with previous results. The characteristic widths of the valence bands and the amount

TABLE II. Energies of conduction states at high symmetry points relative to the calculated Fermi energy, compared with SEE data. Energies in eV.

State	Expt.[a] results	EXH present work	Painter and Ellis [b]	Bassani and Parravicini [c]	Corbato [d]
Γ^+_{3u}	7.7±0.5	8.0	7.5	3.0	11.0
Γ^-_{2g}	12.2±0.5	12.1	10.5	9.0	12.8
Q^+_{1u}	8.7±0.5	19.1	8.0	8.2	9.6

[a] Reference 35.
[b] Reference 77.
[c] Reference 76.
[d] Reference 75.

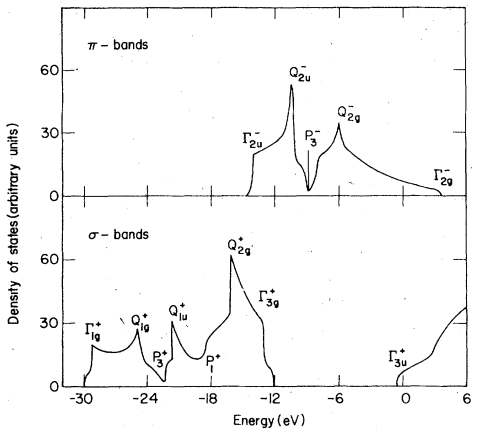

FIG. 5. Partial density of states of graphite.

of $\sigma-\pi$ band overlap at the zone center are given in Table III. Coulson's[70] analysis of the soft x-ray spectroscopy data of Chalkin[30] suggests a width of 5.0 ± 0.5 eV for the π-valence subband, in agreement with the present calculation. The experimental determination of the total valence bandwidth is rather controversial. Early K-emission results of Chalkin[30] suggest a value of about 15-17 eV while ESCA results of Thomas *et al.*[31] and of Hamrin *et al.*[33] suggest values of 31 ± 2 and 30 eV, respectively. The soft x-ray emission spectra arise mainly from the $2p$ part of the valence band (due to the $2p\rightarrow1s$ selection rule for K emission), while the ESCA spectra gives more weight to the $2s$ part (a cross-section ratio $\sigma_{2s}/\sigma_{2p}\approx13$ has been suggested).[126] The value obtained by Chalkin is thus a lower bound to which the $2s$ part of the spectrum (with contributions from the vicinity of the Γ_{1g}^{+} point) should be added. The large width of the observed ESCA bands was attributed[31,33] to the presence of surface impurities such as oxygen whose traces are directly detected in the spectra. Recent x-ray emission spectra of pure graphite obtained by Muller *et al.*[32] indicate a width of 22 eV for the valence band while the new x-ray photoemission data of McFeely[34] yield a value of 24 eV in reasonable agreement with the present calculation. The energetic overlap between valence σ and π bands has also been speculatively established from various experiments. Oscillator-strength sum rules for π and σ transitions indicate a rough overlap of 1–3 eV,[23,28] while analysis of soft x-ray data[30,70] suggests an overlap of about 1.6 eV. The valence $\sigma-\pi$ overlap observed in simple aromatic molecules is of the order of 1 eV.[116]

Several x-ray photoelectron spectra[33,34] and emission[32] spectra of graphite, have been reported. Although direct comparison between x-ray photoelectron and emission spectra with the calculated profile is complicated by the need to weight the latter by the energy dependent transition probabilities,[126] the peak positions and the general features are rather unaffected. In Table IV we have compared the various features obtained in the combined experimental x-ray photoelectron[33] and emission[30,34] spectra with the theoretical assignment based on our calculated density of states. The exact position of our calculated peaks and their parentage was determined by the procedure outlined in Eq. (16). The energies of the calculated values are given relative to the theoretical Fermi energy as yielded by each author. The results of the present work are in very good agreement with experiment and in moderate agreement with the results of Painter and Ellis,[77] while the calculated results of Bassani and Parravicini[76] reveal systematically lower binding energies. Owing to very pronounced cross section effects the occurrence of the relative minima at ~10 and at ~14 eV in our density of states near the P_1^+ and P_3^+ points, respectively, cannot be verified by direct comparison with experiment and it is not sure whether it is an artifact of the calculation model, or not. The maximum intensity in the experimental photoelectron spectra is observed at the peak assigned to the Q_{1u}^{+} point and at the flat top of the $\Gamma_{1g}^{+}-Q_{1g}^{+}$ peak, while in the

TABLE III. Partial valence bandwidths (W_π and W_σ), total valence bandwidth ($W_{\rm tot}$), and σ-π band overlaps ($\Delta\sigma-\pi$) as obtained in various calculations. Energy given in eV.

Property	EXH present work	Painter and Ellis [a,d]	Bassani and Parravicini [b]	Corbato [c]
W_π	5.6	7.35, [c]8.0[d]	5.0	9.8
W_σ	17.0	14.5, [c]16[d]	11.3	16.6
$W_{\rm tot}$	21.2	19.3, [c]20.7[d]	13.8	18.5
$\Delta_{\sigma-\pi}$	1.4	2.7, [c]3.0[d]	1.3	6.0

[a] Reference 77.
[b] Reference 76.
[c] Reference 75.
[d] Reference 35, extended basis set.

TABLE IV. Characteristic features of the valence density of states in graphite. Energies measured relative to the Fermi level, in eV.

Experimental feature	Energy	Theoretical assignment (Present work)	Energy (present work)	Painter and Ellis [a]	Bassani and Parravicini [b]
π-band peak	3-4 [c]	Q_{2u}^{-} saddle point	2.5	2–3	1.5
Top of σ valence band	4 [d]	Γ_{3g}^{+}	4.2	4.5	2.6
σ-band peak	8 ± 1 [d]	Q_{2g}^{+} saddle point	7.2	7.5	5.5
Sharp peak	13.8,[d] 13.0[e]	Q_{1u}^{+} saddle point	13.1	14.2	11.3
Local minima	12–13.8[d]	deep near P_3^{+}	13.6	14.0	12.5
Small peak	17 [e]	Q_{1g}^{+}	16.2	15.5	13.3
Flat region	17–20 [d]	$\sim Q_{1g}^{+} - P_3^{+}$	17–21	~13–15	~12–14
Bottom of valence band	24,[d] 22 [f]	Γ_{1g}^{+}	21.2	19.3, 20.7 [g]	13.8

[a] Reference 77.
[b] Reference 76.
[c] K-emission spectra, Ref. 30.
[d] X-ray photoemission, Ref. 34.
[e] X-ray photoemission, Ref. 33.
[f] X-ray emission spectra, Ref. 32.
[g] Reference 35.

density of states, the Q_{2g}^{+} peak is more intense. Examination of the calculated unit cell charges at the Q_{1u}^{+} point $[(q_{\mu}^{c1}(\vec{k},j) + q_{\mu}^{c2}(\vec{k},j)]$ (see Appendix A) reveals 24% $2s$ character and 76% $2p$ character. The Q_{2g}^{+} state, on the other hand, around which a high density of states is accumulated, is a pure $2p$ state. Using the estimated cross section ratio for $2s$ and $2p$ atomic contributions to the spectral intensity ($\sigma_{2s}/\sigma_{2p} \approx 13$),[126] one obtains that the Q_{1u}^{+} state should indeed reveal higher intensity than the Q_{2g}^{+} peak, in agreement with experiment. Our assignment agrees with that of McFeely *et al.*[34] except for the 13.8 eV peak. These authors speculate that this peak originates from a *high* density of states near the P_1^{+} point. Our calculation reveals a relatively sharp increase in the band energy near P_1^{+}, and consequently a minima rather than a maxima in the density of states.

C. McClure band parameters

The present band-structure calculation can be used to obtain theoretical estimates of the McClure γ_0 and γ_1 band parameters[37,38] previously used in simple π approximations to fit various Fermi surface and optical data.[37-41] Since the optical behavior at low energies is determined by the band structure at the vicinity of the Q point, while Fermi surface data are determined by the behavior at the $H-P$ line in the three-dimensional zone (perpendicular to the P point at the zone corner), we have determined the corresponding two values for γ_0. The optical parameter $\gamma_0^{\rm opt}$ is directly calculated[72] from the band structure (half of the $\pi - \pi^*$ splitting at Q) to be 2.25 eV. Both γ_1 and $\gamma_0^{\rm Fermi}$ are calculated by numerically fitting a separately performed three-dimensional EXH band structure along the $H-P-H$ line to the analytical formula of $E(k_{HP}, \gamma_1, \gamma_0^{\rm Fermi})$ given by Wallace.[69] This yields effective values of $\gamma_0^{\rm Fermi} = 2.53$ eV and $\gamma_1 = 0.32$ eV. These values are obtained from an all-valence electron calculation using five in-plane neighboring atomic shells and considering the interaction of a given plan with its nearest neighbor planes. In π tight-binding calculations retaining nearest neighbors only, a single value is obtained for γ_0. McClure[38] obtained values of $\gamma_0^{\rm Fermi} = 2.8 \pm 0.1$ eV and $\gamma_1 = 0.27$ eV from a fit of a simplified π band structure with only nearest-neighbor interactions to the observed high-temperature diamagnetic susceptibility and the de Haas–van Alphen effect. Cyclotron resonance data fitted by Nozieres[89] yield $(\gamma_0^{\rm Fermi})^2/\gamma_1 = 25$ eV, compared with McClure's value of 29 eV and our value of 20 eV. Magnetoreflection data of Dresselhaus and Mavroides[41] give $\gamma_1 = 0.395$ eV. Long-wavelength and uv optical experiments have yielded $\gamma_1 = 0.14$ eV[22] and $\gamma_1 \cong 0.40$ eV,[23,29] while the ultraviolet optical spectra of the lowest Q-saddle point transition suggest $\gamma_0^{\rm opt} = 2.25-2.4$ eV.[23,24,72]

The electronic contribution to the heat capacity of graphite has been calculated by Bowman and Krumhansl[42] using the π-band-structure parameters of Wallace.[69] Using the γ_0 and γ_1 effective parameters determined in the present study (average values of $\gamma_0^{\rm opt}$ and $\gamma_0^{\rm Fermi}$ were employed) and

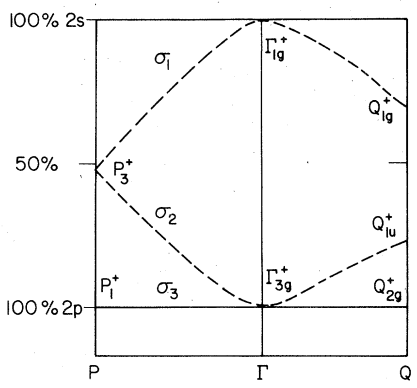

FIG. 6. 2s character of the three lowest valence σ bands along P-Γ-Q directions.

assuming a value of 0.02 eV for the shift of the Fermi level relative to the center of gravity of the π bands at H,[37,42] we obtain $C_{\text{elec}} = 0.43 \times 10^{-5}$ cal mol^{-1} K^{-2} compared with the experimental values[42,43] of 0.6×10^{-5}.

Although the agreement obtained is rather favorable, it should be noted that this merely reflects the fact that the overall level distribution around the Fermi energy in our model is correct, and thus, it probably does not constitute a sensitive test to the adequacy of the theoretical Fermi surface.

D. Charge distribution and bonding

We next turn to consider the charge distribution in the valence band of graphite. A carbon atom in its "reactive" state has an electronic configuration $2s^{1.0}2p_x^{1.0}2p_y^{1.0}2p_z^{1.0}$, or using the notation appropriate for a crystal field with reflection symmetry σ_h in the xy plane: $2s^{1.0}2p_\sigma^{2.0}2p_\pi^{1.0}$. This corresponds to the usually assumed sp^2 hybridization in planar carbon systems. The total orbital valence charges calculated from the band structure using the four occupied valence bands and 180 inequivalent $\vec{k}$ points in the irreducible BZ [$P^{\alpha\alpha}_{\mu\mu}(n)$ in Eq. (A6)] comes out to be $2s^{1.0876}2p_\sigma^{1.9124}2p_\pi^{1.0000}$ which corresponds to a total electronic charge [Q_α in Eq. (A9)] of 4.0000e with σ hybridization of $sp^{1.76}$ which is close to the commonly accepted ideal sp^2 hybridization. When the total valence orbital charges are broken into separate contributions from the individual bands [R^α_μ in Eq. (A7)] it is observed that the lowest valence band (denoted σ_1) contributes most of the 2s charge having the configuration $(2s^{0.7664}2p_\sigma^{0.2346}2p_\pi^{0.0})_{\sigma_1}$ while the next two σ bands (σ_2 and σ_3) give rise to the configuration $(2s^{0.3212}2p_\sigma^{1.6784}2p_\pi^{0.0})_{\sigma_2,\sigma_3}$. The π band has the electronic configuration $(2s^{0}2p_\sigma^{0}2p_\pi^{1.000})_\pi$. Thus, most of the σ covalent bonding in the solid occurring due to $s-p$ overlap, comes from the two highest σ bands.

The band orbital charge itself can be decomposed into contributions from various parts of the Brillouin zone [$q^\alpha_\mu(\vec{k},j)$ in Eq. (A6)]. This is shown in Fig. 6 where the dispersion of the $2s-2p_\sigma$ character of the three valence σ bands along the $P-\Gamma-Q$ directions is revealed. The σ_1 band changes from a pure 2s Bloch state at the zone center to about $\frac{1}{2}$ and $\frac{2}{3}$ 2s character at the P and Q points, respectively. The σ_2 band reveals an opposite behavior, being a pure $2p_\sigma$ Bloch state at the zone center and gaining some 2s character at the P and Q. The third σ_3 band is a pure $2p_\sigma$ Bloch state throughout the $P-\Gamma-Q$ directions. The band-by-band orbital charge representation throughout the BZ shown here, should be viewed as the solid-state analog of the molecular charge decomposition used in quantum chemistry.[92-94] A two-dimensional real-space representation of the charge density contributed by each band at a given point in the BZ is easily obtained when the $2s-2p$ mixing coefficients are given as in Fig. 6.

The "bond order" concept introduced by Coulson for describing π bonding effects can be identified in our calculation scheme by $P^{\alpha,\beta}_{\pi,\pi}(0,n)$ which denotes the charge-density coefficient relating the π wave-function amplitudes of the two translationally inequivalent atoms α and β that are separated by n unit cells. Calculating these values from our eigenvectors, we obtain $P^{c_1,c_2}_{\pi,\pi}(0,0) = 0.525$, $P^{c_1,c_2}_{\pi,\pi}(0,2) = -0.183$, and $P^{c_1,c_2}_{\pi,\pi}(0,3) = -0.052$. The value at $P^{c_1,c_2}_{\pi,\pi}(0,0)$ can be compared with the value of 0.662 obtained for the benzene molecule,[127] indicating a 52.5% double-bond character in the former case [$P^{\pi,\pi}_{c_1c_2}(0,0) = 1$ corresponds to a 100% double bond]. The negative values for the bond order of distant separated atoms, indicate "antibonding" nodal character.

E. Equilibrium unit-cell parameters and bond energy

The unit-cell parameters of graphite under static equilibrium are calculated by minimizing the total crystal energy per unit cell, as a function of the unit cell parameter a. This minimization procedure, carried out using the steepest-descent technique [Eq. (11)] yields $a_{\text{eq}} = 2.482$ Å corresponding to a carbon-carbon bond length of 1.435 Å, which is in only moderate agreement with the experimental value of 1.42 Å (experimental unit cell parameter $a = 2.46$ Å).[124] The cohesive energy is obtained from the total energy per atom at equilibrium, after subtracting from it the sum of free-atom orbital energies and the promotion energy E_{pro} gained by the atom when it returns to its ground $(2s^2 2p^2)\,^3P$ electronic configuration.

The latter energy has been calculated by Goldfarb and Jaffe[128] to be 6.93 eV and by Jordan and Longuet-Higgins[129] to be 7.61 eV. These yield cohesive energies E_c of 8.73 and 8.05 eV, respectively. It is interesting to observe that using the two special $\vec{k}$ points for the hexagonal two-dimensional BZ calculated by Cunningham,[21] instead of the 180 $\vec{k}$ points in the irreducible zone, we obtained an error of only 1.1% in the cohesive energy relative to the dense mesh results, while the six-point representation already yields an error of only 0.2%. No direct experimental determinations of the cohesive energy of graphite are available. The sublimation energy of graphite at 298 °K was determined to be $E_s = 7.4$ eV.[48-50] Adding to this zero-point energy (calculated from the phonon density of states of Young and Koppel[45] to be 0.18 eV) one obtains a value of 7.58 eV for the static energy. Since an average of $\frac{3}{2}$ bonds are involved in the sublimation process,[7] the experimental bond energy per atom is $\frac{2}{3}(E_s + E_{\text{pro}}) = 9.7-10.3$ eV or $E_B = 4.85-5.15$ eV per bond (using $E_{\text{pro}} = 6.93$ eV[128] and $E_{\text{pro}} = 7.61$ eV,[129] respectively). This compares well with the calculated value of $\frac{2}{3}(E_c + E_{\text{pro}}) = 10.44$ eV or $E_B = 5.22$ eV per bond. Independent estimates can be obtained from surface energies. If we denote by $1/\sqrt{3}dR_0$ the number of bonds per unit area involved in creation of two c surfaces, where $d = 3.3$ Å is the interlayer distance, the surface energy σ_c is given by $\frac{1}{2}E_B/\sqrt{3}dR_0$. Using the measured σ_c value of 4800 erg/cm^2,[130] one obtains a bond energy of 4.9 eV which is in reasonable agreement with the presently calculated value and with that published previously.[13]

The contribution of the π valence band to the cohesive energy was calculated by integrating the π energy band over the occupied part of the zone. This yields a stabilization of 2.28 eV coming from this band above. Early π electron calculation on graphite using only nearest-neighbor interaction revealed a π binding energy of 1.08γ,[70] where γ is the resonance integral. Comparison with our results of a full band-structure calculation yields an effective value of $\gamma = 2.09$ eV. This can be compared with various empirical estimates previously suggested, such as $\gamma = 3.0$ eV,[70] and $\gamma = 2.5$ eV.[131] Most of the binding in the crystal results from the σ bands. The greatest contributions to the cohesive energy from these bands were calculated to arise from the vicinity of the BZ points P and Q. At these points the stabilization of the energy bands relative to the atomic energy levels (field stabilization) is high and $s-p$ hybridization is very pronounced (Fig. 6). At the Γ point $s-p$ hybridization is low, resulting in a low crystal-field effect.

The carbon-carbon symmetric stretching force constant was computed from differentiation of the total energy curve at the minimum with respect to the carbon-carbon distance. This yields $k = 5.6 \times 10^5$ dyn/cm. This can be compared with the corresponding values for the benzene molecule $k = 6.71 \times 10^5$ dyn/cm[45] and the naphthalene molecule $k = 4.789 \times 10^5$ dyn/cm.[46] The latter values were used in calculations for the phonon spectrum of graphite[45,46] yielding very good agreement with the measured heat-capacity data and phonon dispersion curves.[47]

F. Behavior under pressure

The effect of external hydrostatic pressure on the band structure of the two-dimensional graphite was investigated by repeating the band calculation for various values of the unit cell parameter a. Figure 7(a) shows the variation of some high-symmetry energy levels with the carbon-carbon distance $R_0 = (1/\sqrt{3})a$ and Fig. 7(b) exhibits a similar plot of the total and π valence bandwidths (W_{tot} and W_π, respectively) and the onset of $\pi \rightarrow \pi^*$ and $\sigma \rightarrow \sigma^*$ band to band transitions ($Q_{2u}^- \rightarrow Q_{2g}^-$ and $\Gamma_{3g}^+ \rightarrow \Gamma_{3u}^+$, respectively). It is interesting to note that upon compression, the bonding Γ_{2u}^- level, representing the lower edge of the π valence subband, is stabilized while the upper edge of the σ subband, the Γ_{3g}^+ antibonding state increases in energy thereby increasing the $\sigma-\pi$ overlap. For lower densities ($R_0 \simeq 1.50$ Å) these bands exchange their order and the $\sigma-\pi$ overlap vanishes. The $\sigma-\pi$

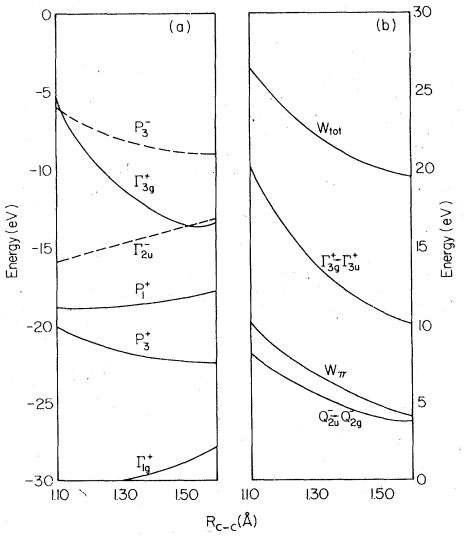

FIG. 7. Dependence of some electron energies at high-symmetry points (a) and the bandwidth, the onsets of $\sigma \rightarrow \sigma^*$ and $\pi \rightarrow \pi^*$ transitions (b) on the interatomic distance.

band splitting ($E_{\Gamma_{2u}^-} - E_{\Gamma_{3g}^+}$) is a measure of the departure from degeneracy between the in-plane $2p_x$ and $2p_y$ orbitals (forming the Γ_{3g}^+ level) and the out-of-plane $2p_z$ orbitals (forming the Γ_{2u}^- level), these orbitals being degenerate in spherically symmetric free carbon state. In layered hexagonal crystals having atoms of different electronegativity in the unit cell (e.g., hexagonal boron nitride[86]) this $\sigma-\pi$ overlap is small due to the larger stability of the Γ_{3g}^+ level, while in small aromatic molecules it is of the order of 1–2 eV.[115-117] The ionization potential of graphite ($-E_{P_3^-}$) is shown to be reduced upon compression, reaching for a compression of 22% about 70% of its value in equilibrium under zero pressure. Similarly, the onsets of the $\sigma \to \sigma^*$ and $\pi \to \pi^*$ transitions are greatly increased by compression of the lattice, the latter transition exhibiting a lower sensitivity due to the relatively low value of the $2p_z - 2p_z$ overlap. Experiments on the optical properties of graphite under high pressure or high temperature could be useful for elucidating the interesting features of $\sigma-\pi$ band interchange and other effects introduced by the variation of the lattice constants.

IV. SUMMARY

The extended-Hückel approximation to the LCAO matrix elements was used to calculate the electronic properties of the two-dimensional graphite. The band structure is shown to agree favorably with previously published first-principles calculations for the valence bands and the low-energy part of the conduction bands. The calculated properties compared with experimental data, are: (a) Interband transition energies (compared with optical data). (b) Energy of high symmetry points in the valence bands (compared with ESCA data). (c) Energy of high symmetry points in the conduction bands (compared with SEE data). (d) Dielectric $\epsilon_{2\perp}(0,\omega)$ function. (e) Density of states (compared with the general features of the soft x-ray emission and ESCA spectra). (f) Effective values for the McClure γ_0 and γ_1 band parameters (used to fit experimental Fermi surface data and optical data through the Slonzewski and Weiss model). (g) The parameter yielding the electronic contribution to the specific heat in the Bowman and Krumhansl model. (h) Equilibrium unit cell parameters of graphite (compared with x-ray data). (i) Cohesive energy (compared with thermochemical estimates). (j) Symmetric vibration stretching force constants (compared with the value used in lattice-dynamical calculations on graphite to obtain good fit with the experimental phonon heat capacity and with the phonon dispersion curves from neutron diffraction).

The behavior of the band structure for various values of the unit-cell parameters as well as the contribution of various bands and points in the Brillouin zone to the orbital charges, are also discussed. The overall success of the extended-Hückel method in accounting for the wealth of experimental data on regular graphite, seems to justify its use also for further investigation on point defect problems in graphite (following article).[19]

APPENDIX A: ORBITAL AND ATOMIC CHARGE DEFINITIONS

We give here briefly the working definitions of orbital and atomic charges used in this work. To avoid arbitrary partitioning of two-center charge terms to equal parts, we transform our eigenvalue problem

$$F(\vec{k})\,C(\vec{k}) = S(\vec{k})\,C(\vec{k})\,\epsilon(\vec{k}) \tag{A1}$$

in the overlapping basis set [$F(\vec{k})$, $S(\vec{k})$, and $C(\vec{k})$ are Fock, overlap, and eigenvector coefficients matrices, respectively] to an orthogonal eigenvalue problem

$$\tilde{F}(\vec{k})\,\tilde{C}(\vec{k}) = \epsilon(\vec{k})\,\tilde{C}(\vec{k}) \tag{A2}$$

using the Löwdin transformation

$$\tilde{F}(\vec{k}) = S^{-1/2}(\vec{k})\,F(\vec{k})\,S^{-1/2}(\vec{k}); \quad \tilde{C}(\vec{k}) = S^{-1/2}(\vec{k})\,C(\vec{k}). \tag{A3}$$

The crystal wave functions $\Psi_j(\vec{k},\vec{r})$ [Eq. (2)] are given now in the orthogonalized Bloch representation $\tilde{\Phi}_\mu^\alpha(\vec{k},\vec{r})$ by:

$$\Psi_j(\vec{k},\vec{r}) = \sum_\mu \sum_\alpha \tilde{C}_{\mu j}^\alpha(\vec{k})\,\tilde{\Phi}_\mu^\alpha(\vec{k},\vec{r}). \tag{A4}$$

The elements of the crystalline charge matrix are given by:

$$P_{\mu\nu}^{\alpha\beta}(n,m) = \frac{1}{\Omega}\int_{BZ} d\vec{k} \sum_{j=1}^{\sigma_{occ}} n_j \tilde{C}_{\mu j}^\alpha(\vec{k})\,\tilde{C}_{\nu j}^\beta(\vec{k})\,e^{i\vec{k}\cdot(\vec{R}_n - \vec{R}_m)} \tag{A5}$$

where Ω is the BZ volume, σ_{occ} is the number of occupied bands in the ground state, and the integration is defined on the occupied part of the BZ.

The charge contributed by the μth basis function on band j at point $\vec{k}$ in the BZ, $q_\mu^\alpha(\vec{k},j)$ is related to the diagonal element of the charge matrix by:

$$P_{\mu\mu}^{\alpha\alpha}(n) = \frac{1}{\Omega}\int_{BZ} d\vec{k} \sum_{j=1}^{\sigma_{occ}} q_\mu^\alpha(\vec{k},j). \tag{A6}$$

The contribution of the jth band to the μ-orbital charge is given by:

$$R^{\alpha}_{\mu j} = \frac{1}{\Omega} \int_{BZ} d\vec{k}\, q^{\alpha}_{\mu}(\vec{k}, j) \tag{A7}$$

and the contribution of the jth band to the total electronic charge, on site α, in the ground state, is given by

$$D^{\alpha}_{j} = \sum_{\mu=1}^{\sigma} R^{\alpha}_{\mu j}. \tag{A8}$$

The BZ integration in Eqs. (A5)–(A8) is replaced by a numerical quadrature over 180 $\vec{k}$ points in the $\frac{1}{12}$ segment of the BZ. The sum of D^{α}_{j} over the sites α that are nearest neighbors to a vacant site (where j denotes here the defect band), is taken as a measure of the localization of the defect charge density (paper II).

The total electronic charge on site α due to all occupied bands, in the ground state, is given by:

$$Q_{\alpha} = \sum_{\mu=1}^{\sigma} P^{\alpha\alpha}_{\mu\mu} \tag{A9}$$

and is equal to the atomic valence charge ($4e$) if no charge transfer takes place. The net atomic charge on site α is given simply by the unscreened charge:

$$q_{\alpha} = Z_{\alpha} - Q_{\alpha}, \tag{A10}$$

where Z_{α} is the core charge (+4 for carbon) on site α. For neutral isolated atoms and for an atom in a homonuclear solid where all sites are crystallographically equivalent, q_{α} is zero.

---

*Present address: Department of Physics, Northwestern University, Evanston, Illinois 60201.

[1]G. F. Koster and J. C. Slater, Phys. Rev. 95, 1167 (1954); 96 1208 (1954).

[2]J. Callaway and A. J. Hughes, Phys. Rev. 156, 860 (1967); 164, 1043 (1967).

[3]F. Bassani, G. Iadonisi, and B. Preziosi, Phys. Rev. 186, 735 (1969).

[4]M. Lannoo and P. Lenglart, J. Chem. Phys. Solids 30, 2409 (1969).

[5]M. Jaros and S. F. Ross, J. Phys. C 6, 1753 (1973); 6, 3451 (1973).

[6]C. A. Coulson and M. J. Kearsley, Proc. R. Soc. A 241, 433 (1957).

[7]C. A. Coulson, M. A. Herrnaes, M. Lead, E. Santos, and S. Senent, Proc. R. Soc. A 274, 461 (1963).

[8]T. Yamaguchi, J. Phys. Soc. Jpn. 17, 1359 (1962); 18, 368 (1963).

[9]C. Kittel and A. H. Mitchell, Phys. Rev. 96, 1488 (1954).

[10]W. Kohn and J. M. Luttinger, Phys. Rev. 97, 1721 (1955); 98, 915 (1955).

[11]F. P. Larkins, J. Phys. Chem. Solids 4, 3065 (1971); 4, 3077 (1971).

[12]R. P. Messmer and G. D. Watkins, Phys. Rev. B 7, 2568 (1973).

[13]A. Zunger, J. Phys. C 6, 72 (1974); 6, 96 (1974).

[14]A. Zunger, J. Chem. Phys. 63, 1713 (1975).

[15]G. D. Watkins and R. P. Messmer, in *Computational Methods for Large Molecules and Localized States in Solids*, edited by F. Herman, A. D. McLean, and R. K. Nesbel (Plenum, New York, 1973), p. 133.

[16]T. F. Lee and T. C. McGill, J. Phys. C 6, 3438 (1973).

[17]A. Zunger, J. Chem. Phys. 62, 1861 (1975).

[18]A. Zunger and A. Katzir, Phys. Rev. B 11, 2378 (1975).

[19]A. Zunger and R. Englman, following paper, Phys. Rev. B 17, 642 (1977).

[20]D. J. Chadi and M. L. Cohen, Phys. Rev. B 7, 692 (1973); 8, 5747 (1973).

[21]S. L. Cunningham, Phys. Rev. B 10, 4988 (1974).

[22]W. S. Boyle and P. Nozières, Phys. Rev. 111, 782 (1958).

[23]E. A. Taft and H. R. Philipp, Phys. Rev. 138, A197 (1965).

[24]S. Ergum, J. B. Yasinsky, and J. R. Towsend, Carbon 5, 403 (1967).

[25]D. L. Greenaway, G. Harbeke, F. Bassani, and E. Tosatti, Phys. Rev. 178, 1340 (1969).

[26]R. Klucker, M. Skobowski and W. Steinmann, Phys. Status Solidi B 65, 703 (1974).

[27]K. Zeppenfeld, Phys. Lett. A 25, 335 (1967).

[28]E. Tosatti and F. Bassani, Nuovo Cimento 65, 161 (1970).

[29]G. Guizetti, L. Nosenzo, E. Reguzzoni, and G. Samoggia, Phys. Rev. Lett. 31, 154 (1973).

[30]F. C. Chalkin, Proc. R. Soc. A 194, 42 (1948).

[31]J. M. Thomas, E. L. Evans, M. Barber, and P. Swift, Trans. Faraday Soc. 67, 1875 (1971).

[32]J. M. Muller, F. Feser, G. Wiech, and A. Faessler, Phys. Lett. A 44, 263 (1973).

[33]K. Hamrin, G. Johansson, U. Gelius, C. Nordling, and K. Siegbahan, Phys. Scr. 1, 277 (1970).

[34]F. R. McFeely, S. P. Kowalczyk, L. Ley, R. G. Cavell, R. R. Pollak, and D. A. Shirley, Phys. Rev. B 9, 5268 (1974).

[35](a) R. F. Willis, B. Feuerbacher, and B. Fitton, Phys. B 4, 2441 (1971). (b) R. F. Willis, B. Fitton, and G. S. Painter, Phys.Rev. B 9, 1926 (1974).

[36]R. F. Willis and B. Fitton, J. Vac. Sci. Technol. 9, 651 (1972).

[37]J. W. McClure, Phys. Rev. 108, 612 (1957).

[38]J. W. McClure, Phys. Rev. 119, 606 (1960).

[39]P. Nozières, Phys. Rev. 109, 1510 (1958).

[40]T. Uda, H. Ushio, and Y. Uemura, J. Phys. Soc. Jpn. 36, 653 (1974).

[41]M. S. Dresselhaus and J. G. Mavroides, IBM J. Res. Develop. 8, 262 (1964); Carbon 1, 263 (1964).

[42]J. C. Bowman and J. A. Krumhansl, J. Phys. Chem. Solids 6, 367 (1958).

[43]P. H. Keesom and N. Pearlman, Phys. Rev. 99, 1119 (1955).

[44]W. De Sorbo and G. E. Nicholas, J. Phys. Chem. Solids 6, 352 (1958).

[45]J. A. Young and J. U. Koppel, J. Chem. Phys. 42, 357 (1965).

[46]K. K. Mani and R. Ramani, Phys. Status Solidi B 61, 659 (1974).

[47]G. Dolling and B. N. Brockhouse, Phys. Rev. 128, 1120 (1962).

[48]G. Glocker, J. Chem. Phys. 22, 159 (1954).
[49]H. T. Knight and J. P. Rink, J. Chem. Phys. 29, 449 (1958).
[50]P. D. Zavitsanos and G. A. Carlson, J. Chem. Phys. 59, 2966 (1973).
[51]G. Wagoner, *Proceedings of the Fourth Conference on Carbon* (Pergamon, New York, 1960), p. 197.
[52]K. A. Muller, Phys. Rev. 123, 1550 (1961).
[53]S. Toyoda, T. Yamakawa, K. Kobayashi, and Y. Yamada, Carbon 10, 646 (1971).
[54]R. W. Henson and W. N. Reynolds, Carbon 3, 277 (1965).
[55]E. Pluchery, *Proceedings of the Conference on Irradiation Damage in Solids and Reactor Materials* (IAEA, Venice, 1962), p. 523.
[56]P. R. Goggin, R. W. Henson, A. J. Perks, and W. N. Reynolds, Carbon 1, 189 (1964).
[57]T. Iwata and T. Nihira, Phys. Lett. 23, 631 (1966).
[58]G. L. Montet, Carbon 11, 89 (1973).
[59]D. T. Eggen, North American Aviation Report, NAA-SR-69 (1960) (unpublished).
[60]T. Iwata and Y. Sato, J. Phys. Soc. Jpn. 23, 1425 (1967).
[61]M. A. Kanter, Phys. Rev. 107, 655 (1957).
[62]C. Baker and A. Kelly, Nature 193, 235 (1962).
[63]P. A. Thrower, Philos. Mag. 18, 697 (1968).
[64]E. W. J. Mitchell and M. R. Taylor, Nature 208, 638 (1965).
[65]G. Hennig, J. App. Phys. 36, 1482 (1965).
[66]G. H. Kinchin, J. Nuclear Energy 1, 124 (1954).
[67]J. E. Hove, in *Proceedings of the First and Second Conference on Carbon* (Buffalo Univ., New York, 1956), p. 25.
[68]W. Primak and L. H. Fuchs, Phys. Rev. 103, 541 (1956).
[69]R. Wallace, Phys. Rev. 71, 622 (1947).
[70]C. A. Coulson and H. Taylor, Proc. R. Soc. A 65, 815 (1952).
[71]J. C. Slonczewski and P. R. Weiss, Phys. Rev. 109, 272 (1958).
[72]L. J. Johnson and G. Dresselhaus, Phys. Rev. B 7, 2275 (1973).
[73]M. Tsukada, K. Nakao, Y. Uemura, and S. Nagai, J. Phys. Soc. Jpn. 32, 54 (1972).
[74]M. Lomer, Proc. R. Soc. A 227, 330 (1955).
[75]F. J. Corbato, in *Proceedings of the Third Conference on Carbon* (Pergamon, London, 1959), p. 173.
[76]F. Bassani and G. P. Parravicini, Nuovo Cimento 50, 95 (1967).
[77]G. S. Painter and D. E. Ellis, Phys. Rev. B 1, 4747 (1970).
[78]J. Zupan, Phys. Rev. B 6, 2477 (1972).
[79]W. Van Haeringen and H. G. Junginger, Solid State Commun. 7, 1723 (1969).
[80]R. P. Messmer, B. McCarrol, and C. M. Singal, J. Vac. Sci. Techno. 9, 891 (1972).
[81]G. Kapsomenos, Ph.D. thesis (Universite Catholique de Louvain, 1972) (unpublished).
[82]R. Hoffman, J. Chem. Phys. 39, 1392 (1963).
[83]D. J. Stukel, R. N. Euwema, T. C. Collins, F. Herman, and R. L. Kortum, Phys. Rev. 179, 740 (1969).
[84]W. E. Rudge, Phys. Rev. 181, 1024 (1969).
[85]A. Zunger, Solid State Commun. 11, 1727 (1972).
[86]A. Zunger and A. Katzir, and A. Halperin, Phys. Rev. B 13, 5560 (1976).
[87]G. Blyholder and C. A. Coulson, Theor. Chim. Acta 10, 316 (1968).
[88]L. C. Allen and J. D. Russel, J. Chem. Phys. 46, 1029 (1967).
[89]T. L. Gilbert, in *Sigma Molecular Orbitals*, edited by O. Sinanoglu and K. B. Wiberg (Yale U.P., New Haven, Conn., 1970), p. 249.
[90]P. O. Löwdin, J. Chem. Phys. 18, 365 (1950).
[91]P. J. Davis and P. Rabinowitz, *Numerical Integration* (Blaisdell, Waltham, 1967).
[92]R. S. Mulliken, J. Chem. Phys. 23, 1033 (1955).
[93]P. Ros and G. C. A. Schmit, Theor. Chim. Acta 4, 1 (1966).
[94]E. W. Stout and P. Politzer, Theor. Chim. Acta 12, 379 (1968).
[95]M. Mizuno and S. Saeki, Mol. Phys. 24, 219 (1972).
[96]M. Pollak and R. Rein, J. Chem. Phys. 47, 2045 (1967).
[97]K. H. Wheelock, H. B. Jonassan, and L. C. Cusachs, Int. J. Quant. Mech. 4, 209 (1971).
[98]B. L. Kalman, J. Chem. Phys. 59, 5184 (1973).
[99]D. C. Carrol, A. T. Armstrong, and S. P. McGlynn, J. Chem. Phys. 44, 1865 (1966).
[100]R. Rein, H. Fukuda, H. Win, G. A. Clark, and F. E. Harris, in *Quantum Aspects of Heterocyclic Compounds in Chemistry and Biochemistry*, Proceedings of the Jerusalem Symposium (Israel Academy of Science and Humanities, Jerusalem, 1969), p. 86.
[101]M. Wolfsberg and L. Helmholtz, J. Chem. Phys. 20, 837 (1952).
[102]H. Basch, A. Viste, and H. B. Gray, Theor. Chim. Acta 3, 358 (1965).
[103]L. C. Cusachs and J. W. Reynolds, J. Chem. Phys. 43, S160 (1965).
[104]C. C. Roothaan, J. Chem. Phys. 19, 1445 (1951).
[105]A. Breeze, P. M. Magee, and P. G. Perkins, J. Non-Cryst. Solids 13, 140 (1974).
[106]M. A. Whitehead, in *Sigma M. O. Theory*, edited by O. Sinanoglu and K. B. Wiberg (Yale U.P., New Haven, Conn., 1970), p. 49.
[107]A. T. Armstrong, B. Bertus, and S. P. McGlynn, Spect. Lett. 1, 43 (1968).
[108]F. P. Boer, M. D. Newton, and W. M. Lipscomb, Proc. Natl. Acad. Sci. U.S. 52, 890 (1964); J. Am. Chem. Soc. 88, 2353 (1966).
[109]O. Sinanoglu and M. K. Orloff, in *Sigma Molecular Orbitals* edited by O. Sinanoglu and K. B. Wiberg (Yale U.P., New Haven, Conn., 1970), p. 390.
[110]R. G. Parr, in *Quantum Theory of Molecular Electronic Structure* (Benjamin, New York, 1963).
[111]R. Pariser, J. Chem. Phys. 21, 568 (1953).
[112]C. K. Jørgensen, S. M. Horner, W. E. Hatfield, and S. Y. Tyrel, Int. J. Quant. Chem. 1, 191 (1967).
[113]M. Lannoo, Phys. Rev. B 10, 2544 (1974).
[114]B. J. Duke, Theor. Chim. Acta 9, 260 (1968).
[115]B. O. Johnsson and E. Lindholm, Ark. Fys. 10, 1 (1968).
[116]H. Bock and W. Fuss, Angew. Chem. 83, 169 (1971).
[117]S. D. Peyerimhof and R. J. Bunker, Theor. Chim. Acta 19, 1 (1970).
[118]R. Rein, N. Fukuda, H. Win, G. A. Clark, and F. E. Harris, J. Chem. Phys. 45, 4743 (1966).
[119]W. J. Hehre, R. F. Stewart, and J. A. Pople, J. Chem. Phys. 51, 7657 (1964).

[120]I. Shavitt, in *Methods in Computational Physics*, edited by B. Alder, S. Frenbach, and M. Rotenberg (Academic, New York, 1963), Vol. 2, p. 1.
[121]S. Srebrenic, H. Weinstein, and R. Paunz, Chem. Phys. Lett. 20, 81 (1973).
[122]F. E. Harris, L. Kumar, and H. Moukhorst, Phys. Rev. B 7, 2850 (1973).
[123]J. Delhale and J. M. Andre, in Proceedings of the NATO Advanced Study Institute on the Electronic Structure of Polymers and Molecules, Namur, 1974 (unpublished)
[124]G. E. Bacon, Acta Cryst. 4, 558 (1951).
[125]V. S. Fomenko, *Handbook of Thermionic Properties* (Plenum, New York, 1966).
[126]U. Gelius, *Electron Spectroscopy*, edited by D. A. Shirley (North Holland, Amsterdam, 1972), p. 314.
[127]C. A. Coulson, *Valence* (Oxford U.P., Oxford, 1961), p. 270.
[128]I. J. Goldfarb and H. H. Jaffe, J. Chem. Phys. 30, 1672 (1959).
[129]P. C. H. Jordan and H. C. Longuet-Higgins, Mol. Phys. 5, 121 (1962).
[130]J. Abrahamson, Carbon 11, 337 (1973).
[131]J. C. Phillips, Rev. Mod. Phys. 42, 317 (1970).